International Journal of Concrete Structures and Materials

RESEARCH Open Access

Eco-Friendly 3D-Printed Concrete Using Steel Slag Aggregate: Buildability, Printability and Mechanical Properties

Nhi Tran[1,2], Mien Van Tran[1,2*], Phuong Tran[3], An Khanh Nguyen[1,2] and Cuong Quoc Nguyen[1,2]

Abstract

Utilizing steel slag aggregate (SA) as a substitute for river sand in 3D concrete printing (3DCP) has emerged as a new technique as natural resources become increasingly scarce. This study investigates the feasibility of using steel slag (SS) as fine aggregate for 3DCP. Ninety mixtures with varying steel slag aggregate-to-cement ratios (SA/C), water-to-cement ratios (W/C), and silica fume (SF) contents were designed to study the workability and compressive strength of the 3D-printed concrete. Additionally, the actual components were printed to evaluate the printability of these mixtures. The experimental results indicate that it is feasible to fully employ SA in concrete for 3D printing. Mixtures with slump values ranging from 40 to 80 mm and slump flow values varying from 190 to 210 mm are recommended for 3D printing. The optimal mix is determined to have SA/C and W/C ratios of 1.0 and 0.51, respectively, and an SF content of 10% by cement weight. A statistical approach was utilized to construct the prediction models for slump and slump flow. Moreover, to predict the plastic failure of the 3D-printed concrete structure, the modified prediction model with an SA roughness coefficient of 4 was found to fit well with the experimental data. This research provides new insights into using eco-friendly materials for 3D concrete printing.

Keywords 3D concrete printing, Eco-friendly materials, Steel slag aggregate, Workability, Printability, Multiple linear regression analysis

1 Introduction

Digital fabrication techniques such as additive manufacturing of concrete (AMoC) or 3D concrete printing (3DCP) have shown the potential to be used in the construction industry and have been under development for the last few decades. Without the requirement of formwork, 3DCP employs a layer-by-layer deposition manner to construct concrete elements directly from the CAD models (Panda et al., 2018). The adoption of 3DCP brings substantial benefits such as enabling architecture flexibility, enhancing productivity, reducing human resources, minimizing material wastage, and lowering the project cost when compared to conventional construction methods (Lyu et al., 2021; Panda et al., 2018; Rehman & Kim, 2021).

For large-scale construction, various 3DCP technologies have been utilized. These technologies are mainly based on two printing techniques, including extrusion-based and powder-based (Nematollahi et al., 2017). Particularly, contour crafting and concrete printing are the two extrusion-based techniques that are commonly used in 3DCP (van Woensel et al., 2018). In concrete extrusion, a structure is generated layerwise by applying a specific pressure to deposit fresh cementitious

Journal information: ISSN 1976-0485 / eISSN 2234-1315.

*Correspondence:
Mien Van Tran
tvmien@hcmut.edu.vn
[1] Faculty of Civil Engineering, Ho Chi Minh City University of Technology (HCMUT), 268 Ly Thuong Kiet Street, District 10, Ho Chi Minh City 70000, Vietnam
[2] Vietnam National University Ho Chi Minh City, Linh Trung Ward, Thu Duc District, Ho Chi Minh City 70000, Vietnam
[3] School of Engineering, RMIT University, Bundoora, VIC 3001, Australia

material along a defined path through a nozzle (Paolini et al., 2019). The extrusion-based printing process is influenced by a number of crucial parameters, such as pumpability, extrudability, and buildability. The fresh concrete should not have particle segregation to prevent blockages (pumpability). In addition, it is required to be extrudable with high shape retention quality (extrudability). Furthermore, it also needs to develop strong green strength to support the subsequently deposited layers without significantly deforming the bottom layers (buildability) (Khan et al., 2020; Nguyen-Van et al., 2023). To this end, in the fresh state, concrete characteristics, such as the mix proportions, the addition of admixtures, rheological properties, open time, and setting time, need to be chosen appropriately or evaluated carefully. Simultaneously, in the hardened state, mechanical properties, such as compressive strength, flexural strength, and shrinkage, should be taken into consideration (Buswell et al., 2018; Krishnaraja & Guru, 2021).

Concrete is one of the most widely used man-made materials by volume in the construction industry due to its standout performance (Khan et al., 2021). Concrete is a mixture of fine and coarse aggregates, cement, admixtures, and water, so it consumes a great deal of natural resources. The explosion of infrastructure and urbanization in recent years has resulted in the over-exploitation of these natural resources, particularly river sand. This might have detrimental effects on the ecosystem. Consequently, it is essential to reduce the reliance on natural resources and find an alternative (Liu et al., 2022). Furthermore, the emissions of solid waste from agriculture, the mining industry, and concrete production continue to increase year after year. Typically, these wastes will be dumped into landfills, putting a burden on our environment. Various types of solid waste, such as mining tailings (Álvarez-Fernández et al., 2021; Ma et al., 2020; Zhou et al., 2023), steel slag (Dai et al., 2021), recycled sand (De Vlieger et al., 2023; Ding et al., 2020), recycled glass (Ting et al., 2019), and waste tires (Sambucci et al., 2023), have been utilized as substitutes for river sand in 3DCP.

Steel slag (SS), a by-product of the steel-making process, is generated when impurities are extracted from steel using lime (CaO), dolomite (MgO), and other supplementary materials. It makes up approximately 15–20% of the mass of steel production (Han et al., 2015). Due to the growing demand for steel, the amount of SS is likely to increase. The accumulation of SS not only occupies a large area of landfills, but also causes harm to the surrounding environment. Therefore, promoting the usage of SS in construction applications is recommended (Pan et al., 2019).

The utilization of SS depends on both its physical and chemical properties. The main chemical compounds found in SS are SiO_2, CaO, Fe_2O_3, Al_2O_3, and MnO and the major mineral components of SS are C_3S, C_2S, C_4AF, RO phase, and free-CaO (Gencel et al., 2021). SS powder has hydraulic properties, and its hydration process is similar to that of cement. This allows for its incorporation into raw meal for clinker production (Cao et al., 2019; Tsakiridis et al., 2008), partial replacement of conventional clinker in blended cement (Cao et al., 2019; Snellings et al., 2022; Wang et al., 2022b), and utilization as a substitute for Portland cement or as a mineral additive in concrete mixes (Liu & Wang, 2017; Wang et al., 2022a). The incorporation of SS in the cement production process helps to reduce the sintering temperature of the raw meal, resulting in a decrease in CO_2 emissions (Martins et al., 2021). Additionally, the inclusion of SS powder in concrete mixtures offers advantages in terms of workability, early autogenous shrinkage, and adiabatic temperature rise (Liu & Guo, 2018). Research has demonstrated that SS can be used as either fine or coarse aggregate for concrete according to its physical properties (Liu & Guo, 2018; Yüksel, 2017). Mien Van Tran et al. (2015) found that in high-strength concrete with 100% coarse aggregate replaced by SS, the compressive strength is comparable to that of conventional concrete. Additionally, the durability is improved in terms of chloride penetration resistance and resistivity. Guo et al. (2018) employed SS as fine aggregate in concrete at replacement percentages of 0%, 10%, 20%, 30%, and 40% by volume. The experimental results indicated that the static and dynamic compressive strengths of concrete have improved, and the suggested optimum content of SS as fine aggregate is 20%. In the same vein, Dai et al. (2021) evaluated the printability of 3D-printed mortar using SS as fine aggregate. An actual 3D structure was printed with the optimal value of 25% SS fine aggregate. Due to the improvement in workability and mechanical strength, it was demonstrated that SS is appropriate for 3DCP. Yu et al. (2023) examined the utilization of SS as a substitute for cement in 3DCP. The findings showed that adding 10% of SS to 3D-printed concrete increased its buildability. However, the rheological properties were significantly reduced when this level exceeded 20%. It has been demonstrated that a replacement rate of 20% is beneficial in lowering the cost and environmental impact of 3D-printed concrete while maintaining its mechanical and rheological characteristics in later stages.

Previous studies have suggested that the utilization of SS in 3DCP is feasible and worth studying owing to the upsides of this resource in terms of eco-friendliness, sustainability, and required properties for printability. However, with a whole replacement of river sand by

SA, optimizing the proportion of fresh concrete for 3D printing is one of the primary challenges. The full integration of SA in concrete can also have some potential drawbacks, including volume expansion caused by free calcium oxides and reduced workability due to the high angularity, rough texture, and water absorption properties of the SA (Dong et al., 2021). Therefore, these concerns need to be taken into consideration during the optimization process of the concrete mixture for 3D printing.

This study aims to investigate the potential of using SS as fine aggregate to completely replace river sand for 3DCP. The feasibility and performance of the material were examined in terms of workability, printability, and buildability in the fresh state and mechanical performance in the hardened state. In 3DCP, the printability and buildability of the fresh concrete are key factors determining the success of the printing process. In this study, these rheology properties of the 3D-printed concrete are evaluated by slump and slump flow values. Then, using the experimental data, a multiple linear regression analysis was applied to develop the prediction models for slump and slump flow. The developed models could be employed to solve problems regarding mix design optimization to satisfy 3D printing requirements.

2 Materials and Testing Procedure

2.1 Material Preparation

In this work, ordinary Portland cement (OPC) and silica fume (SF) were used as binding materials. OPC has a fineness of 3690 cm^2/g, whereas SF is much finer, with a fineness of 19.8 m^2/g. The chemical compositions of cement, silica fume, and steel slag are presented in Table 1.

River sand was completely replaced by SA with a fineness module of 2.54. The SS investigated in this research was obtained from an electric arc furnace system. As shown in Table 1, it has a high percentage of ferric oxide and low levels of amorphous silica and free lime owing to the slow cooling in the atmosphere technique. This characteristic makes the SS have very low or no pozzolanic activity when compared with blast furnace slag (BFS), so it can be used as an aggregate substitute in concrete (Gencel et al., 2021). However, the presence of free limes such as CaO and MgO with low activity may cause expansion risk during the cement hydration process. Therefore, it is necessary to make a pre-treatment to stabilize the free lime in SS by spraying these aggregates with water for a month before incorporating them in the 3D printable concrete. Additionally, tests of typical properties related to SA and river sand were performed and compared to assess the feasibility of SS when entirely replacing river sand as fine aggregate in 3D printing concrete. The results of these tests are shown in Table 2.

Table 1 Chemical compositions of cement, silica fume, and steel slag

Chemical composition (% by mass)			
	Cement	**Silica fume**	**Steel slag**
MgO	1.80	0.36	1.70
Al_2O_3	5.82	–	6.12
SO_3	2.12	0.51	0.70
SiO_2	22.40	98.15	16.5
K_2O	–	0.31	–
CaO	61.90	0.33	29.1
Fe_2O_3	4.10	0.23	39.4
P_2O_5	–	–	0.32
TiO_2	–	–	1.04
Cr_2O_3	–	–	1.30
MnO	–	–	4.12
ZnO	–	–	0.30
Loss of ignition	2.10	0.30	

Table 2 Typical properties of river sand and steel slag aggregate

Property	**River sand**	**Steel slag aggregate**
Water absorption, %	0.56	1.92
Dry density, g/cm^3	2.66	3.35
Soundness in magnesium sulfate for 5 cycles, %	4.38	3.96

It is noticeable that the SA has higher water absorption and is significantly heavier than the river sand. The high ferric oxide content contributes to its high density and interconnected pore characteristic, which makes it have a higher water absorption when compared to river sand (Tran et al., 2015). Of the physical properties of aggregates shown in Table 2, the soundness property is crucial to the feasible potential of SA usage in concrete. In this research, the soundness of SA was evaluated in accordance with ASTM C88-13 (2013). This test method involves repeatedly immersing aggregates in saturated solutions of magnesium sulfate to allow the salt solutions to penetrate into the pores of the aggregate. The internal expanding force, generated from the crystallization of salt crystals, mimics the expansion of water on freezing. The soundness of the aggregate is evaluated by determining the weight loss of the test sample. Table 2 shows a comparable soundness between river sand and pre-treated SA, and the pre-treated SA is likely superior to the river sand in terms of soundness. Also, according to ASTM C33 (2018), at which the average weight loss of

the aggregate is not greater than 15% with magnesium sulfate usage, both the river sand and pre-treated SA satisfy the soundness specification for concrete aggregates. This implies a feasible usage of SA to entirely replace river sand in 3D-printed concrete.

In this research, pre-treated SA was sieved into different sizes and combined into grading as shown in Fig. 1. Additionally, a modified polycarboxylate-based superplasticizer (PA) was adopted with a dosage of 1% by cement weight to achieve the required flowability of the printing concrete. In order to evaluate the rheological properties of fresh concrete, a total of 90 concrete mixtures were examined. These mixtures were designed with the steel slag aggregate-to-cement ratios (SA/C) ranging from 1.0 to 1.5 by weight, the water-to-cement ratios (W/C) varying from 0.49 to 0.53, and the silica fume (SF) contents set at 5%, 10%, and 15% by cement weight. The detailed mix proportions used in this study can be found in Table 3.

To prepare the printing mixtures, the binding materials and SA were mixed together for 1 min. Subsequently, three-fourths of the total amount of water along with the PA were added and stirred for 4 min. Finally, the remaining water was added to the mixture with 2 min of mixing until a homogenous state was achieved.

2.2 Slump and Slump Flow Tests

Rheology is an important indicator to assess the printability of 3DCP. To ensure pumpability and extrudability, the fresh concrete must have high workability, with low yield stress and low viscosity. However, after the extrusion process, high yield stress and high viscosity are required so the fresh materials can meet the buildability criteria (Pan et al., 2022). Laskar et al. (2009) has indicated that slump and slump flow values can be connected to rheological parameters. As slump or slump flow increases, yield stress linearly decreases. A relationship also exists between plastic viscosity and slump, as well as slump flow. In this research, slump and slump flow tests were conducted to evaluate the rheology properties of fresh concrete for 3D printing.

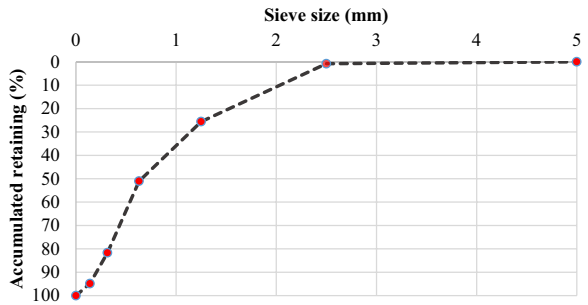

Fig. 1 Sieving analysis of the steel slag

The slump test was carried out using a conical mold in accordance with ASTM C230 (2021). The fresh material was added to the mold in two layers, each of which was tamped 20 times. The excess material was removed by using a steel ruler to flatten the top surface of the mold. Subsequently, the mold was lifted and the difference in height between the mold and the mortar was recorded as the slump value (Fig. 2).

The preparation procedure for the slump flow test according to ASTM C1437 (2020) is similar to the slump test. After the mold was removed, the steel table was dropped 25 times. The diameter of the mortar was measured in two perpendicular directions and the average of these values was defined as the slump flow value (Fig. 3).

2.3 Compressive Test

After conducting the slump and slump flow tests, the fresh concrete was cast into cubic specimens with a size of 50×50×50 mm. All the samples were then cured underwater at an ambient temperature of 27 ± 2 °C and a relative humidity of 90–100%. The compressive strengths of the hardened concrete were tested at the ages of 1 (R1) and 28 days (R28) in accordance with ASTM C109 (2021).

2.4 Printability Assessment

After conducting the slump and slump flow tests, the printability of the mixtures was evaluated by printing hollow squares with a length of 600 mm (Fig. 4). The printed filament had a width and a height of 20 mm and 10 mm, respectively. The printing parameters, including the flow rate, printing speed, and cylinder nozzle diameter, were all fixed at 22 ml/s, 45 mm/s, and 50 mm, respectively. The gantry concrete printer utilized in the actual printing test is shown in Fig. 5. Each printed filament was assessed based on the following requirements (Kazemian et al., 2017):

1) The printed filament has no surface defects, or discontinuity owing to excessive stiffness and insufficient cohesion.
2) The edges of the printed layer must be visible and squared according to the original design.
3) The printed layer must meet the requirements for dimension consistency and conformity.

2.5 A Statistical Approach to Optimize Mixture Designs

In multiple linear regression, the prediction model can be considered as an equation expressing the relationship

Table 3 Concrete mixtures with steel slag aggregate

Mix	SF	SA/C	W/C	C	PA (% by C mass)	Mix	SF	SA/C	W/C	C	PA (% by C mass)
1	0.05	1.0	0.49	1	1	46	0.10	1.3	0.49	1	1
2	0.05	1.0	0.50	1	1	47	0.10	1.3	0.50	1	1
3	0.05	1.0	0.51	1	1	48	0.10	1.3	0.51	1	1
4	0.05	1.0	0.52	1	1	49	0.10	1.3	0.52	1	1
5	0.05	1.0	0.53	1	1	50	0.10	1.3	0.53	1	1
6	0.05	1.1	0.49	1	1	51	0.10	1.4	0.49	1	1
7	0.05	1.1	0.50	1	1	52	0.10	1.4	0.50	1	1
8	0.05	1.1	0.51	1	1	53	0.10	1.4	0.51	1	1
9	0.05	1.1	0.52	1	1	54	0.10	1.4	0.52	1	1
10	0.05	1.1	0.53	1	1	55	0.10	1.4	0.53	1	1
11	0.05	1.2	0.49	1	1	56	0.10	1.5	0.49	1	1
12	0.05	1.2	0.50	1	1	57	0.10	1.5	0.50	1	1
13	0.05	1.2	0.51	1	1	58	0.10	1.5	0.51	1	1
14	0.05	1.2	0.52	1	1	59	0.10	1.5	0.52	1	1
15	0.05	1.2	0.53	1	1	60	0.10	1.5	0.53	1	1
16	0.05	1.3	0.49	1	1	61	0.15	1.0	0.49	1	1
17	0.05	1.3	0.50	1	1	62	0.15	1.0	0.50	1	1
18	0.05	1.3	0.51	1	1	63	0.15	1.0	0.51	1	1
19	0.05	1.3	0.52	1	1	64	0.15	1.0	0.52	1	1
20	0.05	1.3	0.53	1	1	65	0.15	1.0	0.53	1	1
21	0.05	1.4	0.49	1	1	66	0.15	1.1	0.49	1	1
22	0.05	1.4	0.50	1	1	67	0.15	1.1	0.50	1	1
23	0.05	1.4	0.51	1	1	68	0.15	1.1	0.51	1	1
24	0.05	1.4	0.52	1	1	69	0.15	1.1	0.52	1	1
25	0.05	1.4	0.53	1	1	70	0.15	1.1	0.53	1	1
26	0.05	1.5	0.49	1	1	71	0.15	1.2	0.49	1	1
27	0.05	1.5	0.50	1	1	72	0.15	1.2	0.50	1	1
28	0.05	1.5	0.51	1	1	73	0.15	1.2	0.51	1	1
29	0.05	1.5	0.52	1	1	74	0.15	1.2	0.52	1	1
30	0.05	1.5	0.53	1	1	75	0.15	1.2	0.53	1	1
31	0.10	1.0	0.49	1	1	76	0.15	1.3	0.49	1	1
32	0.10	1.0	0.50	1	1	77	0.15	1.3	0.50	1	1
33	0.10	1.0	0.51	1	1	78	0.15	1.3	0.51	1	1
34	0.10	1.0	0.52	1	1	79	0.15	1.3	0.52	1	1
35	0.10	1.0	0.53	1	1	80	0.15	1.3	0.53	1	1
36	0.10	1.1	0.49	1	1	81	0.15	1.4	0.49	1	1
37	0.10	1.1	0.50	1	1	82	0.15	1.4	0.50	1	1
38	0.10	1.1	0.51	1	1	83	0.15	1.4	0.51	1	1
39	0.10	1.1	0.52	1	1	84	0.15	1.4	0.52	1	1
40	0.10	1.1	0.53	1	1	85	0.15	1.4	0.53	1	1
41	0.10	1.2	0.49	1	1	86	0.15	1.5	0.49	1	1
42	0.10	1.2	0.50	1	1	87	0.15	1.5	0.50	1	1
43	0.10	1.2	0.51	1	1	88	0.15	1.5	0.51	1	1
44	0.10	1.2	0.52	1	1	89	0.15	1.5	0.52	1	1
45	0.10	1.2	0.53	1	1	90	0.15	1.5	0.53	1	1

Fig. 2 Measurement of slump value of 3D-printed concrete using SA

Fig. 3 Measurement of slump flow value of 3D-printed concrete using SA

between dependent and independent variables. In this study, the dependent variables were slump and slump flow, whereas the independent variables were SF content, SA/C ratio, and W/C ratio. Equation (1) shows a basic

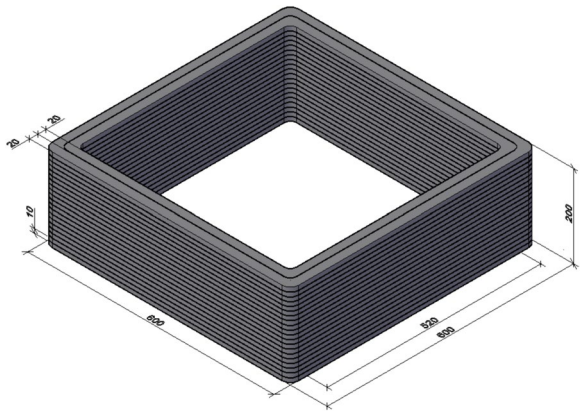

Fig. 4 Illustration of the printed sample for the printability assessment (dimensions in millimeters)

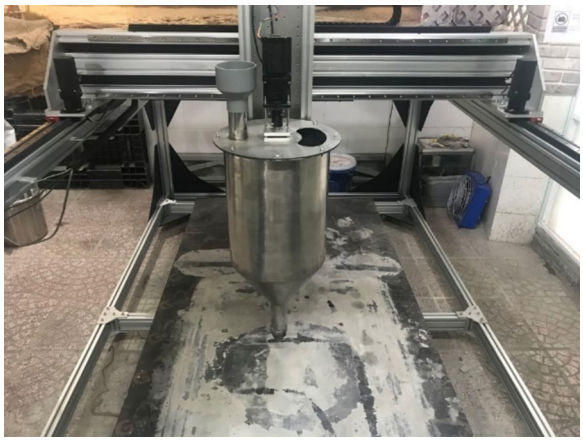

Fig. 5 The gantry concrete printer used in the actual printing test

multiple linear regression with three quantitative independent variables:

$$\mathrm{E}(\mathrm{y}) = \beta_0 + \beta_1 \mathrm{x}_1 + \beta_2 \mathrm{x}_2 + \beta_3 \mathrm{x}_3 \quad (1)$$

where β_0 is the y-intercept, β_i is the partial regression coefficient, which represents the regression coefficient of x_i when all other independent variables are held fixed, and x_i is the independent variable.

An important assumption of the linear regression model is that there is "no interaction" among independent variables, which means the impact of one independent variable on the dependent variable will not be affected by others.

The steps to statistically optimize mixture designs are presented as follows:

- Analysis of variance (ANOVA) was utilized to identify whether there are interactions among independent variables and whether the independent variables have an effect on the dependent variables.

- Multiple linear regression models were generated for each dependent variable (slump and slump flow) depending on the independent variables (SF content, SA/C ratio, and W/C ratio).
- Model validation using adjusted R-square ($R^2_{Adjusted}$) and F-test.
- The developed models for slump and slump flow could be utilized to solve the optimization problems.

2.6 Buildability Assessment

Buildability is the ability to print components layerwise to a specific level without visual deformation. Kazemian et al. (2017) stated three main causes of deformation, including self-weight, weight of stacked layers, and extrusion pressure. Currently, there is no standard procedure available for determining the buildability of 3D-printed concrete. Numerous researchers evaluated the buildability directly by visual inspection based on the number of layers printed or height achieved in a single printing process without collapse (Joh et al., 2020; Pham et al., 2020; Sun et al., 2020), while others indirectly assessed it through rheological properties and early-age mechanical properties (Jayathilakage et al., 2020; Yuan et al., 2019; Zhang et al., 2018).

In this research, the buildability of mixtures was evaluated by conducting a cylinder stability test utilizing a cylinder with a 40 mm diameter and 80 mm height. The test procedure was carried out referred to Kazemian et al. (2017) and Bong et al. (2021) as follows:

1) The cylinder was fixed in place on a metal plate and two layers of fresh concrete, each 40 mm in height, were filled into the mold.
2) Each layer was tamped 20 times and then the excess material was removed to flatten the top surface of the mold.
3) After the mold was slowly and gently removed, a flat plastic plate was placed on the top of the sample. A load was gradually applied until the cylinder specimen visibly deformed or collapsed. The loading rate was 1 N/min (Fig. 6a).
4) The deformation (i.e., the change in height) of the sample before and after applying load was recorded using a digital camera. The photographs captured were then imported into ImageJ software to calculate the deformation (Fig. 6b).

3 Results and Discussion

3.1 Slump and Slump Flow

As demonstrated in Figs. 7 and 8, the slump and slump flow values rose with either an increase in W/C or a decrease in SA/C.

The increase could be attributed to the mixing water. The mixing water in the concrete mixture includes water for the hydration process to create cement paste and water absorption by aggregates. When the amount of water is low, under the effect of molecular attraction, the water is just enough to adsorb on the surface of the solid particles without creating the workability of the mixture. Additionally, even though SA was saturated before mixing, it still absorbs a certain amount of the mixing water due to its surface structure with numerous open pores. This causes the cement paste to lack water, which reduces the workability of the concrete mix. In contrast, when the water content increases to a specific value, free water will appear and thicken the surface of the solid particles. This lowers the internal friction between them, resulting in higher workability. Another possible explanation for this is that with a higher volume of SA content, there will be greater interaction between the aggregate particles since there is not enough cement to completely cover them. As a result, internal friction will rise and resist the flow. In addition, the rough surface of SA also plays an integral part in the greater friction between the aggregates.

SF can be added to the concrete mixture to increase the plastic viscosity and prevent segregation. The

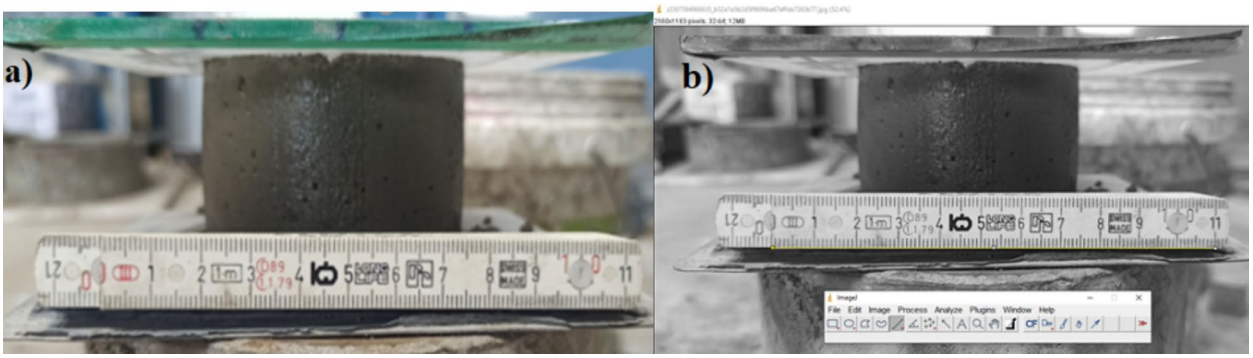

Fig. 6 **a** Cylinder stability test setup, **b** analyzing images utilizing ImageJ software

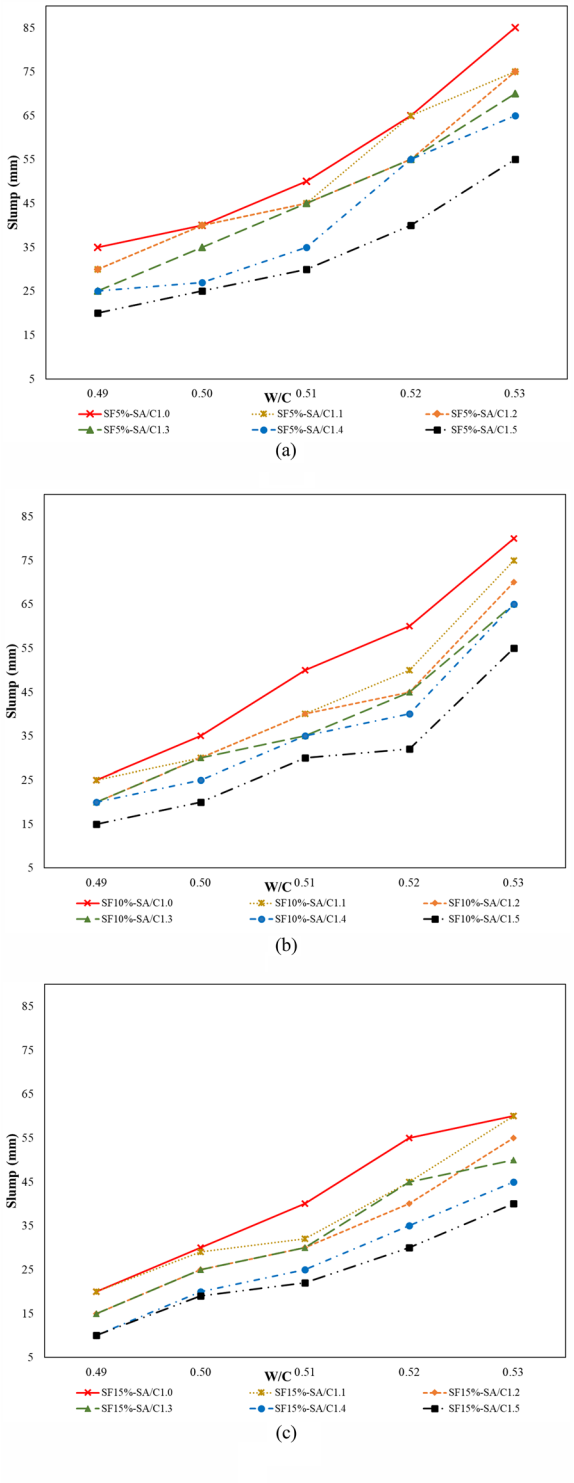

Fig. 7 Effects of SF, SA/C and W/C on slump values of fresh concretes

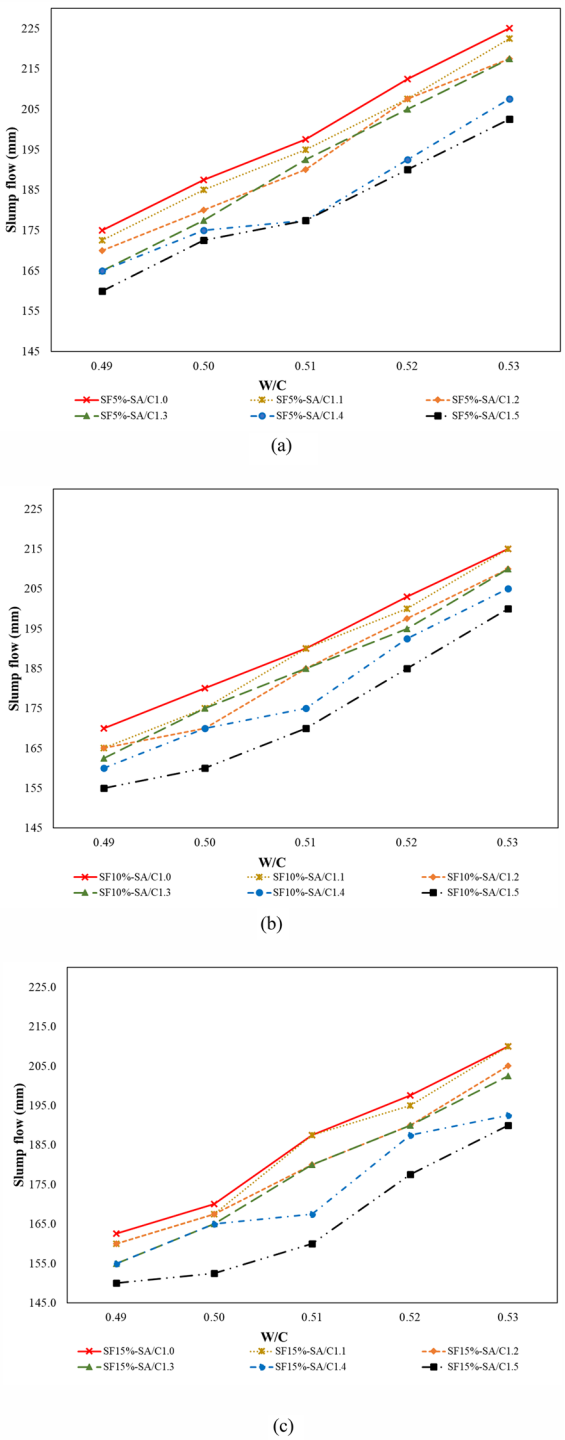

Fig. 8 Effects of SF, SA/C and W/C on slump flow values of fresh concretes

experimental results indicated that slump and slump flow values were shown to be lower as the SF content increased. It is suggested that as the surface area of SF is larger than that of cement, it will absorb more water, leading to a decrease in workability or an increase in plastic viscosity.

3.2 Compressive Strength

Compressive strength improved with an increase in W/C from 0.49 to 0.51, whereas a reduction was observed when this ratio increased further from 0.51 to 0.53 (Fig. 9a). As mentioned earlier, SA has a surface structure with numerous open pores. Despite being saturated before mixing, SA still absorbs a certain amount of the mixing water. When the W/C ratio is less than 0.49, the initial water added is insufficient to allow for a proper hydration process, which results in relatively low compressive strength. However, cement requires 20–22% of mixing water to hydrate, so when the W/C ratio increases from 0.49 to 0.51, there will be a small amount of excess water. The SA partially absorbs the excess water, so the cement has enough water for further hydration. This makes the fresh concrete have suitable plasticity and form a denser structure, which accelerates the compressive strength. However, when the W/C ratio continues to increase further, the higher the W/C ratio, the more water is separated from the fresh mixture. The evaporation of bleeding water from the cement paste during the curing process leads to the formation of porosity in the microstructure of the hardened concrete, reducing the compressive strength.

With the SA/C ratio of 1.1, the compressive strength of 3D-printed concrete was the highest, but in general, with a further increase in the SA/C ratio, the compressive strength decreased (Fig. 9b). It could be reasoned that the surface of SA is rougher than that of river sand, which improves the interaction between the SA and cementitious paste, contributing to the increased compressive strength of concrete. However, SA with high angularity requires more cement than river sand to be effectively coated. When the amount of SA is greater than the amount of cement, the amount of cement is insufficient to completely cover the aggregate particles, causing the aggregate particles to interact and enhancing the dry friction force, which lowers compressive strength. Furthermore, the surface roughness of SA increases its water absorption. Therefore, when more SA is added, this may reduce the hydration of the cementitious material, which could result in poor cohesion between the SA and cement paste, leading to a decrease in compressive strength.

When varying the SF content, the compressive strength was highest at the value of 10% (Fig. 9c). This result could be due to its void-filling ability. The fineness allows SF to fill the micro-pores between the cement particles, resulting in higher bonding strength between the aggregate and the cement paste and reducing the segregation phenomenon. However, when the SF content is increased further to 15%, the excess SF will absorb a significant amount of mixing water due to its large surface area, resulting in insufficient water for the hydration process, which will cause a reduction in the compressive strength of 3D-printed concrete.

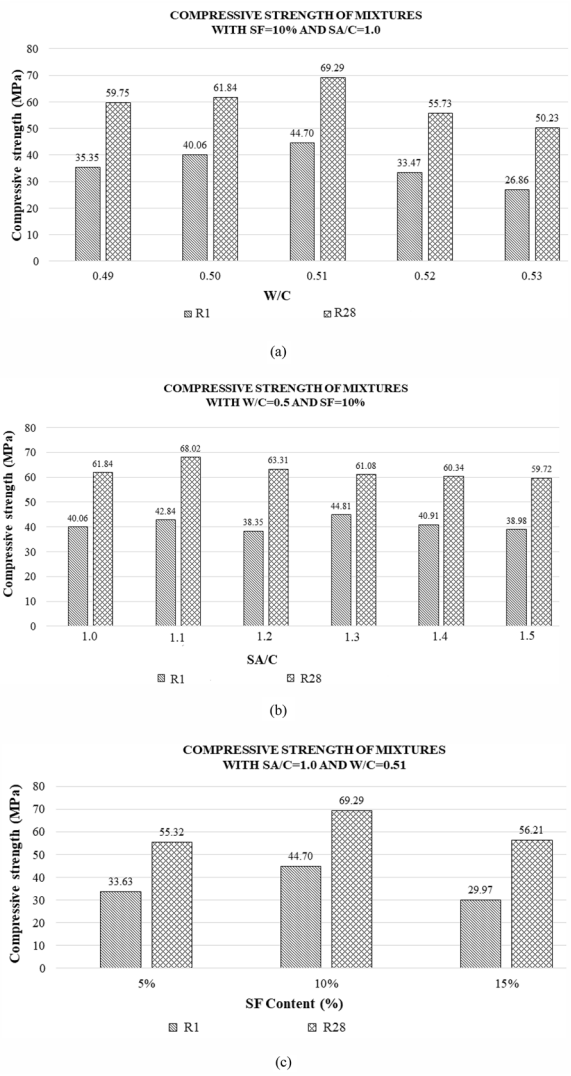

Fig. 9 Compressive strength of mixtures when varying: **a** W/C ratio, **b** SA/C ratio, **c** SF content

3.3 Printability Assessment

Figure 10a illustrates a result in which a mixture with poor workability was disqualified according to the first print quality criteria owing to the detection of discontinuity. The filament had a rough, dry surface and seemed to be disruptively extruded. While a proportion that had SA/C and W/C ratios of 1.0 and 0.51, respectively, and an SF content of 10% achieved the best print quality. The fresh material was flowable with a slump value of 50 mm and a slump flow value of 190 mm. It can be continuously extruded through the nozzle and hold its shape after

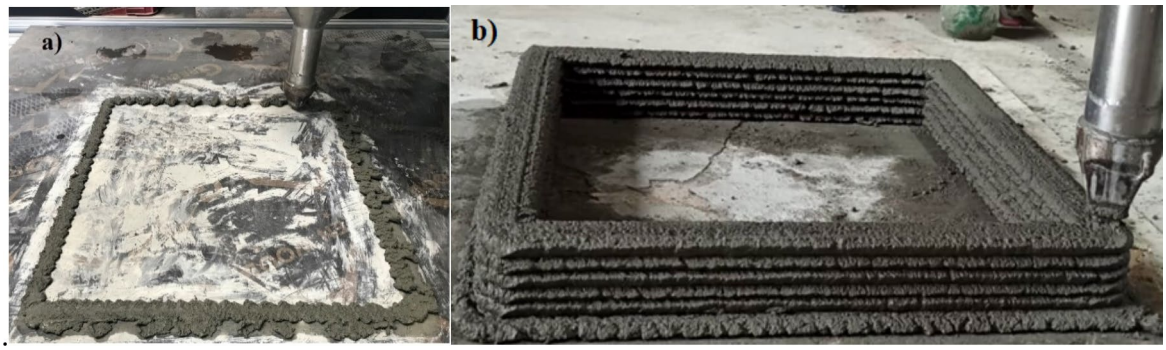

Fig. 10 Visual inspection of deposited filaments: **a** disqualified filament, **b** qualified filament

the extrusion process with a fine and smooth surface (Fig. 10b).

Based on observations of experimental results, other printable mixtures that meet all three print quality requirements are presented in Table 4. Specifically, the mixture with an SF content of 5%, an SA/C ratio of 1.1, and a W/C of 0.52 was slightly pasty with a slump value of 65 mm and a slump flow value of 208 mm. This sample easily flowed through the nozzle; nevertheless, it was still able to ensure shape retention after deposition despite the high slump and slump flow values. Another proportion with SF content, SA/C ratio, and W/C ratio of 15%, 1.3, and 0.52, respectively, was continuously deposited, although it was slightly dry. The deposited filament still ensured dimension consistency and shape retention. These results suggest that a mixture with a slump value between 40 and 80 mm and a slump flow value between 190 and 210 mm is suitable for 3D-printed concrete with SS as fine aggregate.

3.4 Statistical Analysis of Experimental Data and Validation of Multiple Linear Regression Models

Analysis of variance (ANOVA) was conducted to identify correlations among independent variables and the effects of independent variables on dependent variables. ANOVA of experimental data was carried out with the software named SPSS. The Pearson correlation coefficient ($-1 \le r \le +1$) was used to determine the linear correlation level between two quantitative variables. When two variables are significantly linearly related, the absolute value of r approaches 1, whereas when $r=0$, the variables are not linearly connected. Additionally, it is necessary to conduct hypothesis testing to evaluate if the linear correlation can be developed for the entire population. The p-value measures the statistical significance of the correlation coefficient. If the p-value is less than the significance level (0.01 level), then the hypothesis that there is no linear correlation between the two variables will be rejected. As can be seen from Table 5, there are no interactions among independent variables, and all three independent variables have an effect on the dependent variables, especially the W/C ratio, which exhibits significant correlations with slump flow and slump with correlation coefficients of 0.885 and 0.844, respectively.

According to the ANOVA analysis results (refer to Tables 6 and 7), the multiple linear regression models of slump flow and slump were generated and are shown as Eq. (2) and Eq. (3):

Table 4 Printable mixtures

SF	SA/C	W/C	Slump flow (mm)	Slump (mm)	Visual inspection	Compressive strength R1 (MPa)	Compressive strength R28 (MPa)
0.05	1.1	0.52	208	65	Slightly pasty Ensure dimension conformity Ensure shape retention	41.1	54.7
0.10	1.0	0.51	190	50	Flowable Ensure shape retention Fine and smooth surface	44.7	69.3
0.15	1.3	0.52	190	45	Slightly dry Flowable Ensure dimension conformity Ensure shape retention	29.3	53.2

Table 5 Correlations

		SF	SA/C	W/C	Slump flow	Slump
Pearson correlation (*r*)	SF	1	0	0	− 0.281	− 0.322
	SA/C	0	1	0	− 0.332	− 0.348
	W/C	0	0	1	0.885	0.844
	Slump flow	− 0.281	− 0.332	0.885	1	0.967
	Slump	− 0.322	− 0.348	0.844	0.967	1
p-value (2-tailed)	SF		1	1	0.007	0.002
	SA/C	1		1	0.001	0.001
	W/C	1	1		0.000	0.000
	Slump flow	0.007	0.001	0.000		0.000
	Slump	0.002	0.001	0.000	0.000	

** . Correlation is significant at the 0.01 level (2-tailed)

Table 6 Regression analysis result of slump flow

Model summary

Model	R	R-square	Adjusted R-square	Std. error of the estimate
1	0.986[a]	0.973	0.972	3.12073

ANOVA[b]

Model		Sum of squares	df	Mean square	F	*p*-value
1	Regression	30114.07	3	10038	1031	2.87E(-67)
	Residual	837.548	86	9.739		
	Total	30951.62	89			

Coefficients[a]

Model		Unstandardized coefficients		Standardized coefficients	t	*p*-value
			Std. error	Beta		
1	(Constant)	− 349.8	12.136		− 28.823	5.76E(− 46)
	SF	− 1.275	0.081	− 0.281	− 15.823	3.35E(− 27)
	SA/C	− 36.095	1.926	− 0.332	− 18.74	4.12(E-32)
	W/C	1160.833	23.261	0.885	49.906	2.81(E-65)

a. Predictors: (Constant), W/C, SA/C, SF

b. Dependent variable: slump flow

$$E(y)_{slumpflow} = -349.8 - 1.275SF - 36.095S/C + 1160.833W/C, \quad (2)$$

$$E(y)_{slump} = -429.556 - 1.367SF - 35.333S/C + 1033.333W/C, \quad (3)$$

where $E(y)_{slumpflow}$ and $E(y)_{slump}$ are slump flow (mm) and slump (mm), respectively, SF is the silica fume content, SA/C is the steel slag aggregate-to-cement ratio, and W/C is the water-to-cement ratio.

In a linear regression model, a factor is considered to have an impact on the outcome if the *p*-value in the T-test is less than the significance level of 0.05 (0.05 level). From the data in Tables 6 and 7, it is apparent that all the independent variables are statistically significant, with *p*-values for T-tests being less than 0.05.

Figure 11a, b presents the actual values of slump and slump flow (obtained from experiments) against the predicted values (obtained from prediction models).

These graphs illustrate that the relationships between independent variables and dependent variables are effectively represented by the developed models with high R-square values of 0.97 and 0.93. Generally, the R-square value, also known as the coefficient of determination, can

Table 7 Regression analysis result of slump

Model summary						
Model	**R**	**R-square**	**Adjusted R-square**	**Std. error of the estimate**		
1	0.968[a]	0.937	0.934	4.462		
ANOVA[b]						
Model		**Sum of squares**	**df**	**Mean square**	**F**	***p*-value**
1	Regression	25298.83	3	8432.94	423.48	2.23E(− 51)
	Residual	1712.556	86	19.913		
	Total	27011.39	89			
Coefficients[a]						
Model		**Unstandardized coefficients**		**Standardized coefficients**	**t**	***p*-value**
			Std. Error	Beta		
1	(Constant)	− 429.556	17.354		− 24.753	6.92E(− 41)
	SF	− 1.367	0.115	− 0.322	− 11.861	8.58E(− 20)
	SA/C	− 35.333	2.754	− 0.348	− 12.829	1.13E(− 21)
	W/C	1033.333	33.261	0.844	31.067	1.60E(− 48)

a. Predictors: (Constant), W/C, SA/C, SF

b. Dependent variable: slump

be used to quantify how effectively independent variables account for the variance in dependent variables. It has a scale of 0–1, and a higher R-square value shows a better fit of the model to the entire population. However, it is demonstrated that as more independent factors are added to the linear regression model, the coefficient of determination stays unchanged or increases. As a result, the R-square value will rise even if the additional independent variables have no effect on the dependent variables. In this case, the adjusted R-square will better reflect the fit of the multiple linear regression model, as the adjusted R-square will consider whether additional independent variables make a contribution to the model. As shown in Tables 6 and 7, the adjusted R-squares of slump flow and slump models are 0.972 and 0.934, respectively. This indicates that the independent variables account for 97.2% and 93.4% of the variations in the slump flow and slump, respectively. The F-test of overall adequacy determines whether the multiple linear regression model has a better fit for the entire population than a model with no independent variables. It evaluates the hypothesis H_0: $\beta_i = 0$ versus H_1: $\beta_i \neq 0$. It is apparent that the overall significance of the two regression models is satisfied as the *p*-values of the F-tests are considerably less than 0.05 (0.05 level). According to the results of the linear regression analysis, the prediction models of slump and slump slow are robust from a statistical perspective. These models can be utilized for mixture proportion optimization using any suitable optimization tool.

3.5 Buildability Assessment

It can be seen from Fig. 12a, b that the deformation increased when the W/C ratio increased and the SA/C ratio decreased (i.e., the workability increased). As mentioned earlier, after the extrusion process, the fresh concrete should have a high yield stress value in order to have acceptable buildability with less deformation. An inverse relationship also exists between yield stress and workability. Thus, in this case, a rise in the W/C ratio and a fall in the SA/C ratio cause an increase in workability. This leads to lower yield stress, which results in poor buildability of fresh materials. In addition, similarly to conventional concrete, in the case of fresh concrete for 3D printing, the higher content of fine aggregate gives the bulk volume as well as favorable buildability to the printed filament (Ma et al., 2018). In terms of the effect of SF, when the SF content increased (i.e., the workability decreased), the deformation decreased (Fig. 12c). Kazemian et al. (2017) and Zhang et al. (2018) demonstrated that the addition of SF improves the yield stress of fresh concrete, which improves the buildability. Based on the cylinder stability test, mixtures with an SF content of 15%, an SA/C ratio of 1.5, and a W/C ratio ranging from 0.49 to 0.51 will have acceptable buildability with less deformation.

The failure of buildability during the 3DCP process can be detected owing to either elastic buckling or plastic collapse (refer to Fig. 13a, b). The former illustrates the failure caused by the stiffness of concrete, which results in a loss of geometric stability. The latter, on the other hand,

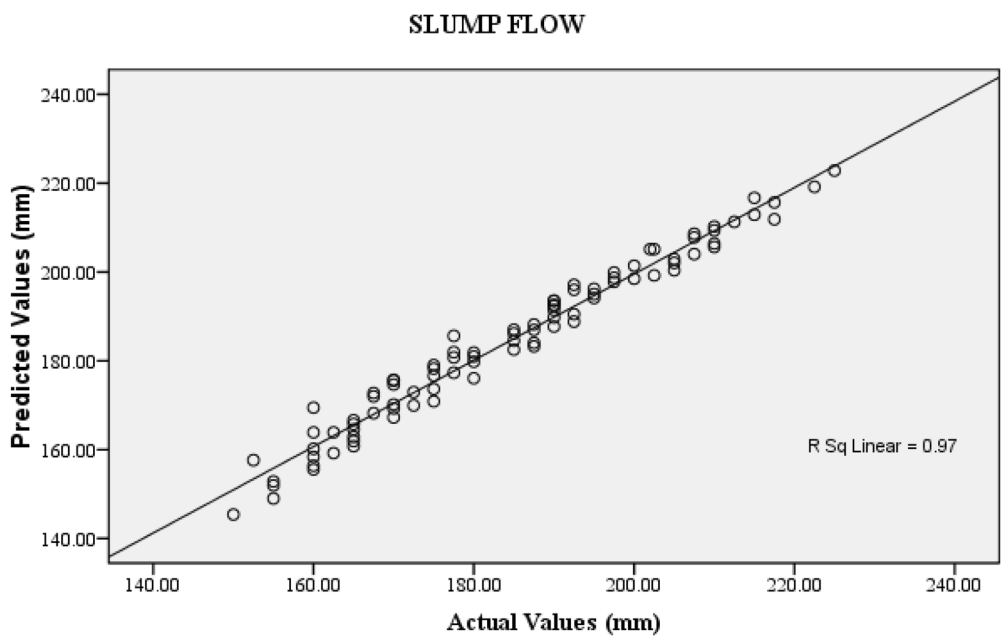

(a)

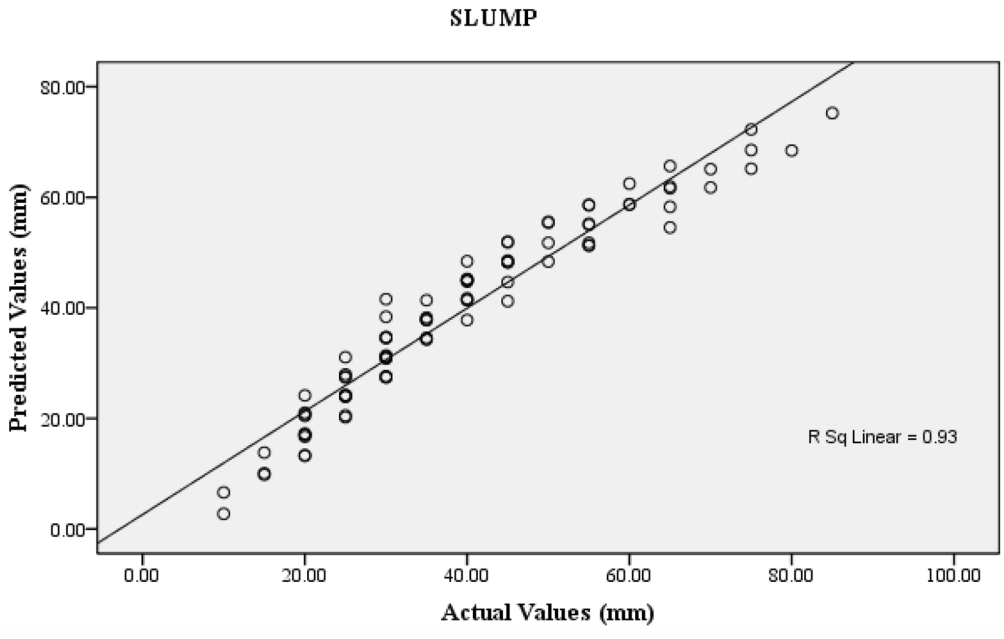

(b)

Fig. 11 Predicted values versus actual values: **a** slump flow, **b** slump

describes a failure when the maximum stress at the bottom layer meets the yield strength of the material as the dead weight loading increases (Suiker et al., 2020).

In order to prevent buildability failures, it is necessary to predict the maximum build height or the failure modes of materials for 3DCP. Numerous researchers have employed numerical simulation approaches, experimental trial-and-error printing methods, and other strategies to gain a better understanding of the structural failure modes of 3D-printed concrete (Casagrande et al., 2020;

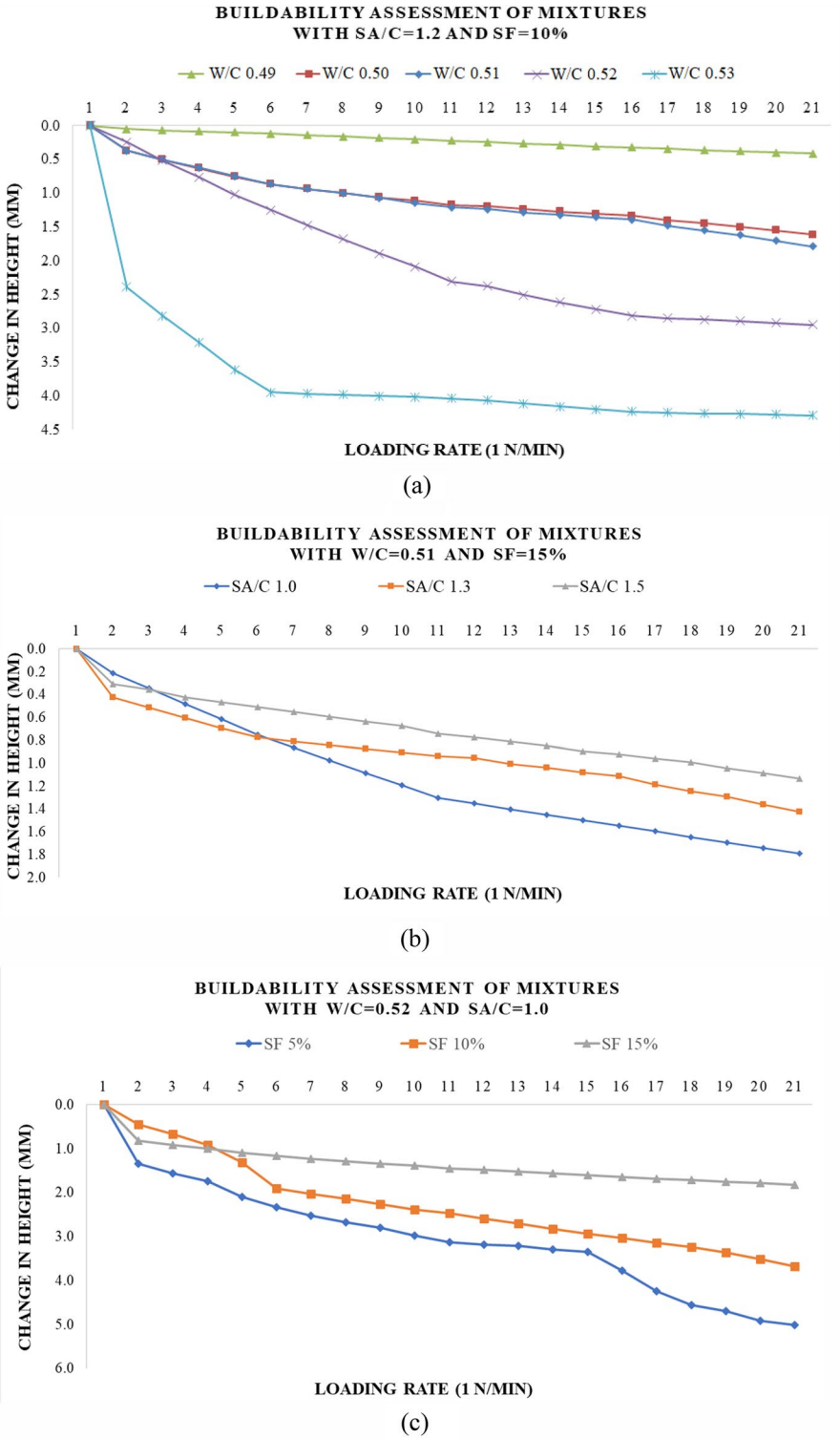

Fig. 12 Buildability assessment results when varying: **a** W/C ratio, **b** SA/C ratio, **c** SF content

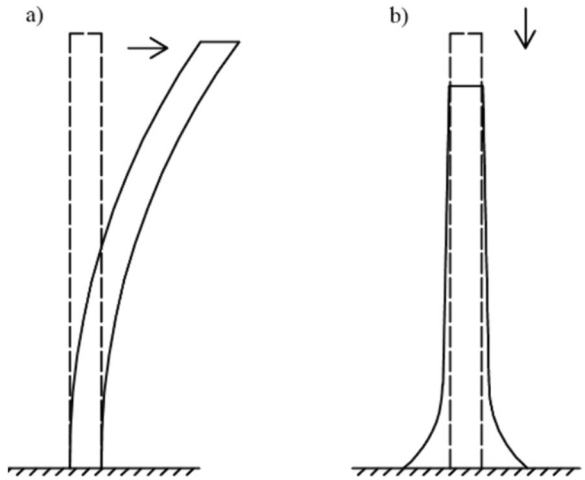

Fig. 13 Buildability failure by: **a** elastic buckling, **b** plastic collapse (modified from (Suiker et al., 2020))

Panda et al., 2019; Roussel, 2018; Wolfs et al., 2018). This study employed the experimental results from the buildability tests with the failure prediction models suggested by Rahul & Santhanam (Rahul & Santhanam, 2020) to examine the occurrence of both elastic buckling and plastic collapse. The crucial height (H_c) at which plastic collapse could happen is determined by

$$\mathrm{H_c} = \frac{\tau_c(t)}{\rho g}, \tag{4}$$

where $\tau_c(t)$ is the strength of the concrete at the bottom layer at any time t, p is the density of the printing material, and g is the gravitational acceleration.

In addition, the critical height H_c at which elastic buckling failure is expected to occur is defined as:

$$Hc = \left(\frac{8\mathrm{EI}}{\mathrm{pgA}}\right)^{\frac{2}{3}}, \tag{5}$$

where E is the elastic modulus of the material, I is the quadratic moment of inertia, p is the density of the printing material, g is the gravitational acceleration, and A is the cross-sectional area.

Figure 14 shows the competition between experimental results and modeling results of the mixture with SF content of 15%, SA/C and W/C ratios of 1.5 and 0.51, respectively.

It can be seen that elastic buckling had little impact on the buildability failures in this particular case and that the majority of them were caused by plastic collapse. A possible explanation for this might be that elastic buckling does not have much of an impact on buildability failures for low-height printing components, so horizontal deformation was not taken into account

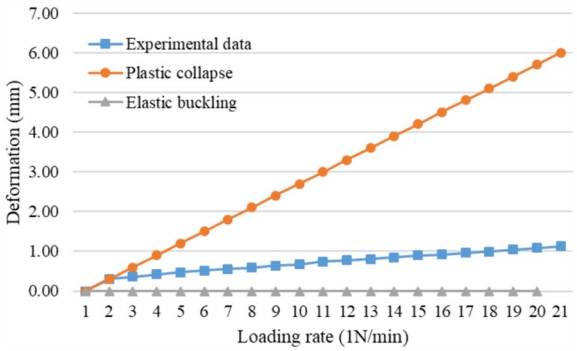

Fig. 14 Measured and predicted deformations of 3D-printed concrete structure

when evaluating buildability failures in this study. The plastic collapse is affected by the yield strength evolution of cementitious material over time. At an early age, the yield strength of fresh concrete increases linearly with time due to flocculation and C–S–H generation. When the hydration process proceeds faster, the yield strength as well as the plastic collapse also increase rapidly. Additionally, the predicted plastic collapse values were significantly higher than the experimental deformation, which may be explained by analyzing the prediction formula. The prediction formula was suggested for concrete using river sand aggregates with relatively round and smooth surfaces; however, when employing SA with rough surfaces, it is required to take the roughness coefficient, N, into consideration. Figure 15 shows the comparison of experimental results and modified modeling results after taking the roughness coefficient into account.

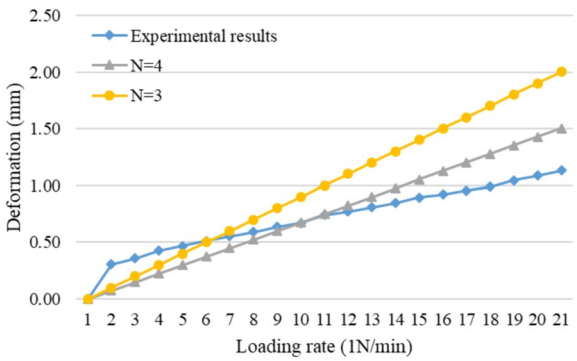

Fig. 15 Comparison of experimental results and modified modeling results

In addition, the paired-samples *T*-test (refer to Table 8) was utilized to evaluate the fit of each model (i.e., $N=3$ or 4) to the experimental data. A paired-samples T-test will examine whether the mean change for these pairs is substantially different from zero.

It can be seen from the data in Table 8 that when comparing the experimental results and the modified modeling results with $N=3$, the *p*-value is less than the standard significance value of 0.05 (0.05 level). This means that there is a statistical difference between experimental and predicted data. Specifically, the average difference is − 0.30004 and the confidence interval of the difference estimates that the actual population difference between the experimental and predicted data is likely between − 0.456 and − 0.144. In contrast, when comparing the experimental results and the modified modeling results with $N=4$, the *p*-value is greater than the standard significance value of 0.05 (0.05 level). This indicates that there is no difference between the paired samples. Thus, the modified prediction model with a roughness coefficient of 4 would fit the experimental data better. As can be seen from Fig. 15, the experimental results at the beginning were greater than the predicted results. It may be that before being loaded, SA particles are coated with cement paste, so they are not in direct contact with each other. However, after being loaded 1–2 times, the cement paste film moves, and the adjacent SA particles begin to come into direct contact with each other. The SA particles with a high roughness surface will generate the internal friction force in the concrete mixture. This phenomenon increases the shear resistance and compression resistance of concrete. As a result, in comparison to the beginning and to the predicted values, the deformation of the sample grows gradually.

4 Conclusions

This study set out to assess the feasibility of utilizing SS as fine aggregate in 3DCP. Three parameters, including the SA/C ratio, the W/C ratio, and SF content, were evaluated for their significance to the properties of 3D-printed concrete, such as slump, slump flow values, compressive strength, printability, and buildability. Based on the experimental results, the following conclusions can be drawn:

- It is feasible to use SA as an entire replacement for river sand to produce a printable 3D concrete.
- As the W/C ratio increases, the workability of fresh material increases, and the compressive strength decreases.
- The workability declines as the SF content increases, and the highest compressive strength is achieved at an SF content of 10%.
- The workability of the fresh concrete using SA depends on the SA content. The higher the SA/C ratio, the lower the workability. It could be caused by the rough surface and angularity of SS, resulting in high water absorption.
- According to the visual inspection of the printability test, it was found that a mixture that has a slump value between 40 and 80 mm and a slump flow value between 190 and 210 mm is suitable for 3DCP employing SS as fine aggregate. Two linear regression models of slump and slump flow were generated and statistically assessed for the feasibility of employing them for mix design optimization:

$$E(y)_{slumpflow} = -349.8-1.275SF-36.095SA/C+1160.833W/C$$

$$\mathrm{E}(y)_{slump} = -429.556-1.367SF-35.333SA/C+1033.333W/C.$$

- To predict the plastic failure of the 3D-printed concrete structure, the modified prediction model with

Table 8 Paired-samples T-test result

Paired-samples test								
	Paired differences					t	df	*p*-value (2-tailed)
	Mean	Std. deviation	Std. error mean	95% confidence interval of the difference				
				Lower	Upper			
Pair 1 Experimental results—$N=3$	− 0.30004	0.343	0.075	− 0.456	− 0.144	− 4.014	20	0.001
Pair 2 Experimental results—$N=4$	− 0.04967	0.192	0.042	− 0.137	0.038	− 1.187	20	0.249

an SA roughness coefficient of 4 was found to fit well with the experimental data.

- Overall, the proportion that has SA/C and W/C ratios of 1.0 and 0.51, respectively, and an SF content of 10% is found to be the optimal eco-friendly mix for 3D printing.

Acknowledgements
We would like to thank Ho Chi Minh City University of Technology (HCMUT), VNU-HCM for the support of time and facilities for this study.

Author contributions
NT: formal analysis, writing—original draft. MVT: conceptualization, methodology, writing—review. PT: editing. AKN and CQN: experiments. All authors read and approved the final manuscript.

Funding
This research received no external funding.

Availability of data and materials
The datasets used and/or analyzed during the current study are available from the corresponding author on reasonable request.

Declarations

Competing interests
The authors declare that they have no competing interests.

Received: 21 March 2024 Accepted: 23 June 2024
Published online: 22 September 2024

References

Álvarez-Fernández, M. I., Prendes-Gero, M. B., González-Nicieza, C., Guerrero-Miguel, D. J., & Martínez-Martínez, J. E. (2021). Optimum mix design for 3D concrete printing using mining tailings: A case study in Spain. *Sustainability, 13*(3), 1–14. https://doi.org/10.3390/su13031568

ASTM C1437-20. (2020). *Standard test method for flow of hydraulic cement mortar* (pp. 6–7). ASTM Int. https://doi.org/10.1520/C1437-20

Astm, C. (2013). *Test Method for soundness of aggregates by use of sodium sulfate or magnesium sulfate* (p. 05). ASTM Stand.

ASTM C109/C109M-21. (2021). *Standard test method for compressive strength of hydraulic cement mortars (Using 2-in. or [50 mm] Cube Specimens)* (p. 12). ASTM Int. https://doi.org/10.1520/C0109_C0109M-21

ASTM C230/C230M-21. (2021). *Standard specification for flow table for use in tests of hydraulic cement* (pp. 1–8). ASTM Int. https://doi.org/10.1520/C0230_C0230M-20

ASTM C33/C33M-18. (2018). *Standard specification for concrete aggregates ASTM C33/C33M-18*. ASTM Stand.

Bong, S. H., Xia, M., Nematollahi, B., & Shi, C. (2021). Ambient temperature cured 'just-add-water' geopolymer for 3D concrete printing applications. *Cement and Concrete Composites*. https://doi.org/10.1016/j.cemconcomp.2021.104060

Buswell, R. A., Leal de Silva, W. R., Jones, S. Z., & Dirrenberger, J. (2018). 3D printing using concrete extrusion: A roadmap for research. *Cement and Concrete Research, 112*(May), 37–49. https://doi.org/10.1016/j.cemconres.2018.05.006

Cao, L., Shen, W., Huang, J., Yang, Y., Zhang, D., Huang, X., Lv, Z., & Ji, X. (2019). Process to utilize crushed steel slag in cement industry directly: Multi-phased clinker sintering technology. *Journal of Cleaner Production, 217*, 520–529. https://doi.org/10.1016/J.JCLEPRO.2019.01.260

Casagrande, L., Esposito, L., Menna, C., Asprone, D., & Auricchio, F. (2020). Effect of testing procedures on buildability properties of 3D-printable concrete. *Construction and Building Materials*. https://doi.org/10.1016/j.conbuildmat.2020.118286

Dai, S., Zhu, H., Zhai, M., Wu, Q., Yin, Z., Qian, H., & Hua, S. (2021). Stability of steel slag as fine aggregate and its application in 3D printing materials. *Construction and Building Materials, 299*, 123938. https://doi.org/10.1016/j.conbuildmat.2021.123938

De Vlieger, J., Boehme, L., Blaakmeer, J., & Li, J. (2023). Buildability assessment of mortar with fine recycled aggregates for 3D printing. *Construction and Building Materials*. https://doi.org/10.1016/j.conbuildmat.2023.130313

Ding, T., Xiao, J., Zou, S., & Wang, Y. (2020). Hardened properties of layered 3D printed concrete with recycled sand. *Cement and Concrete Composites*. https://doi.org/10.1016/j.cemconcomp.2020.103724

Dong, Q., Wang, G., Chen, X., Tan, J., & Gu, X. (2021). Recycling of steel slag aggregate in portland cement concrete: An overview. *Journal of Cleaner Production*. https://doi.org/10.1016/j.jclepro.2020.124447

Gencel, O., Karadag, O., Oren, O. H., & Bilir, T. (2021). Steel slag and its applications in cement and concrete technology: A review. *Construction and Building Materials, 10*(283), 122783.

Guo, Y., Xie, J., Zheng, W., & Li, J. (2018). Effects of steel slag as fine aggregate on static and impact behaviours of concrete. *Construction and Building Materials, 192*, 194–201. https://doi.org/10.1016/j.conbuildmat.2018.10.129

Han, F., Zhang, Z., Wang, D., & Yan, P. (2015). Hydration heat evolution and kinetics of blended cement containing steel slag at different temperatures. *Thermochimica Acta, 605*, 43–51. https://doi.org/10.1016/J.TCA.2015.02.018

Jayathilakage, R., Rajeev, P., & Sanjayan, J. (2020). Yield stress criteria to assess the buildability of 3D concrete printing. *Construction and Building Materials*. https://doi.org/10.1016/j.conbuildmat.2019.117989

Joh, C., Lee, J., Bui, T. Q., Park, J., & Yang, I. H. (2020). Buildability and mechanical properties of 3D printed concrete. *Materials (basel)*. https://doi.org/10.3390/ma13214919

Kazemian, A., Yuan, X., Cochran, E., & Khoshnevis, B. (2017). Cementitious materials for construction-scale 3D printing: Laboratory testing of fresh printing mixture. *Construction and Building Materials*. https://doi.org/10.1016/j.conbuildmat.2017.04.015

Khan, M. S., Sanchez, F., & Zhou, H. (2020). 3-D printing of concrete: Beyond horizons. *Cement and Concrete Research*. https://doi.org/10.1016/j.cemconres.2020.106070

Khan, S. A., Koç, M., & Al-Ghamdi, S. G. (2021). Sustainability assessment, potentials and challenges of 3D printed concrete structures: A systematic review for built environmental applications. *Journal of Cleaner Production, 303*, 127027. https://doi.org/10.1016/j.jclepro.2021.127027

Krishnaraja, A. R., & Guru, K. V. (2021). 3D printing concrete: A review. *IOP Conference Series Materials Science and Engineering, 1055*(1), 012033. https://doi.org/10.1088/1757-899x/1055/1/012033

Laskar, A. I. (2009). Correlating slump, slump flow, vebe and flow tests to rheological parameters of high-performance concrete. *Materials Research, 12*(1), 75–81. https://doi.org/10.1590/S1516-14392009000100009

Liu, J., & Guo, R. (2018). Applications of steel slag powder and steel slag aggregate in ultra-high performance concrete. *Advances in Civil Engineering*. https://doi.org/10.1155/2018/1426037

Liu, J., Nguyen-Van, V., Panda, B., Fox, K., Du Plessis, A., & Tran, P. (2022). Additive manufacturing of sustainable construction materials and form-finding structures: A review on recent progresses. *3D Printing and Additive Manufacturing, 9*(1), 12–34. https://doi.org/10.1089/3dp.2020.0331

Liu, J., & Wang, D. (2017). Influence of steel slag-silica fume composite mineral admixture on the properties of concrete. *Powder Technology*. https://doi.org/10.1016/j.powtec.2017.07.052

Lyu, F., Zhao, D., Hou, X., Sun, L., & Zhang, Q. (2021). Overview of the development of 3D-printing concrete: A review. *Applied Sciences, 11*(21), 9822.

Ma, G., Li, Y., Wang, L., Zhang, J., & Li, Z. (2020). Real-time quantification of fresh and hardened mechanical property for 3D printing material by intellectualization with piezoelectric transducers. *Construction and Building Materials*. https://doi.org/10.1016/j.conbuildmat.2019.117982

Ma, G. W., Wang, L., & Ju, Y. (2018). State-of-the-art of 3D printing technology of cementitious material—an emerging technique for construction. *Science China Technological Sciences, 61*(4), 475–495. https://doi.org/10.1007/s11431-016-9077-7

Martins, A. C., De Carvalho, J. M., Costa, L. C., Andrade, H. D., de Melo, T. V., Ribeiro, J. C., Pedroti, L. G., & Peixoto, R. A. (2021). Steel slags in cement-based composites: An ultimate review on characterization, applications and performance. *Construction and Building Materials, 12*(291), 123265.

Nematollahi, B., Xia, M., & Sanjayan, J. (2017). Current progress of 3D concrete printing technologies. *Proceedings of the International Symposium on Automation and Robotics in Construction (ISARC)*. https://doi.org/10.22260/isarc2017/0035

Nguyen-Van, V., Li, S., Liu, J., Nguyen, K., & Tran, P. (2023). Modelling of 3D concrete printing process: A perspective on material and structural simulations. *Additive Manufacturing, 61*(November 2022), 103333. https://doi.org/10.1016/j.addma.2022.103333

Pan, T., Jiang, Y., & Ji, X. (2022). Interlayer bonding investigation of 3D printing cementitious materials with fluidity-retaining polycarboxylate superplasticizer and high-dispersion polycarboxylate superplasticizer. *Construction and Building Materials*. https://doi.org/10.1016/j.conbuildmat.2022.127151

Pan, Z., Zhou, J., Jiang, X., Xu, Y., Jin, R., Ma, J., Zhuang, Y., Diao, Z., Zhang, S., Si, Q., & Chen, W. (2019). Investigating the effects of steel slag powder on the properties of self-compacting concrete with recycled aggregates. *Construction and Building Materials, 200*, 570–577. https://doi.org/10.1016/j.conbuildmat.2018.12.150

Panda, B., Lim, J. H., & Tan, M. J. (2019). Mechanical properties and deformation behaviour of early age concrete in the context of digital construction. *Composites Part b: Engineering*. https://doi.org/10.1016/j.compositesb.2019.02.040

Panda, B., Tay, Y. W. D., Paul, S. C., & Tan, M. J. (2018). Current challenges and future potential of 3D concrete printing. *Materialwissenschaft Werkst, 49*(5), 666–673. https://doi.org/10.1002/mawe.201700279

Paolini, A., Kollmannsberger, S., & Rank, E. (2019). Additive manufacturing in construction: A review on processes, applications, and digital planning methods. *Additive Manufacturing, 1*(30), 100894.

Pham, L., Tran, P., & Sanjayan, J. (2020). Steel fibres reinforced 3D printed concrete: Influence of fibre sizes on mechanical performance. *Construction and Building Materials*. https://doi.org/10.1016/j.conbuildmat.2020.118785

Rahul, A. V., & Santhanam, M. (2020). Evaluating the printability of concretes containing lightweight coarse aggregates. *Cement and Concrete Composites*. https://doi.org/10.1016/j.cemconcomp.2020.103570

Rehman, A. U., & Kim, J. H. (2021). 3D concrete printing: A systematic review of rheology, mix designs, mechanical, microstructural, and durability characteristics. *Materials, 14*(14), 3800.

Roussel, N. (2018). Rheological requirements for printable concretes. *Cement and Concrete Research*. https://doi.org/10.1016/j.cemconres.2018.04.005

Sambucci, M., Biblioteca, I., & Valente, M. (2023). Life cycle assessment (LCA) of 3D concrete printing and casting processes for cementitious materials incorporating ground waste tire rubber. *Recycling*. https://doi.org/10.3390/recycling8010015

Snellings, R., Machner, A., Bolte, G., Kamyab, H., Durdzinski, P., Teck, P., Zajac, M., Muller, A., de Weerdt, K., & Ben Haha, M. (2022). Hydration kinetics of ternary slag-limestone cements: Impact of water to binder ratio and curing temperature. *Cement and Concrete Research, 151*, 106647. https://doi.org/10.1016/J.CEMCONRES.2021.106647

Suiker, A. S. J., Wolfs, R. J. M., Lucas, S. M., & Salet, T. A. M. (2020). Elastic buckling and plastic collapse during 3D concrete printing. *Cement and Concrete Research*. https://doi.org/10.1016/j.cemconres.2020.106016

Sun, X., Wang, Q., Wang, H., & Chen, L. (2020). Influence of multi-walled nanotubes on the fresh and hardened properties of a 3D printing PVA mortar ink. *Construction and Building Materials*. https://doi.org/10.1016/j.conbuildmat.2020.118590

Ting, G. H. A., Tay, Y. W. D., Qian, Y., & Tan, M. J. (2019). Utilization of recycled glass for 3D concrete printing: Rheological and mechanical properties. *Journal of Material Cycles and Waste Management*. https://doi.org/10.1007/s10163-019-00857-x

Tran, M., Van, C. V., Nguyen, T. N., & Stitmannaithum, B. (2015). Properties of high strength concrete. *Journal of Material Cycles and Waste Management, 4*(263), 121–134. https://doi.org/10.2208/jscej1969.1977.263_121

Tsakiridis, P. E., Papadimitriou, G. D., Tsivilis, S., & Koroneos, C. (2008). Utilization of steel slag for Portland cement clinker production. *Journal of Hazardous Materials, 152*(2), 805–811. https://doi.org/10.1016/J.JHAZMAT.2007.07.093

van Woensel, R., van Oirschot, T., Burgmans, M. J. H., Mohammadi, M., Ph, D., & Hermans, K. (2018). Printing architecture: An overview of existing and promising additive manufacturing methods and their application in the building industry. *The International Journal of the Constructed Environment*. https://doi.org/10.18848/2154-8587/cgp/v09i01/57-81

Wang, Y. S., Lee, H. S., Lin, R. S., & Wang, X. Y. (2022a). Effect of silicate-modified calcium oxide-based expansive agent on engineering properties and self-healing of ultra-high-strength concrete. *Journal of Building Engineering*. https://doi.org/10.1016/j.jobe.2022.104230

Wang, Y. S., Tae, S. H., Lin, R. S., & Wang, X. Y. (2022b). Effects of Na2CO3 on engineering properties of cement–limestone powder–slag ternary blends. *Journal of Building Engineering*. https://doi.org/10.1016/j.jobe.2022.104937

Wolfs, R. J. M., Bos, F. P., & Salet, T. A. M. (2018). Early age mechanical behaviour of 3D printed concrete: Numerical modelling and experimental testing. *Cement and Concrete Research*. https://doi.org/10.1016/j.cemconres.2018.02.001

Yu, Q., Zhu, B., Li, X., Meng, L., Cai, J., Zhang, Y., & Pan, J. (2023). Investigation of the rheological and mechanical properties of 3D printed eco-friendly concrete with steel slag. *Journal of Building Engineering, 72*, 106621. https://doi.org/10.1016/J.JOBE.2023.106621

Yuan, Q., Li, Z., Zhou, D., Huang, T., Huang, H., Jiao, D., & Shi, C. (2019). A feasible method for measuring the buildability of fresh 3D printing mortar. *Construction and Building Materials*. https://doi.org/10.1016/j.conbuildmat.2019.07.326

Yüksel, İ. (2017). A review of steel slag usage in construction industry for sustainable development. *Environment Development and Sustainability, 19*(2), 369–384. https://doi.org/10.1007/s10668-016-9759-x

Zhang, Y., Zhang, Y., Liu, G., Yang, Y., Wu, M., & Pang, B. (2018). Fresh properties of a novel 3D printing concrete ink. *Construction and Building Materials*. https://doi.org/10.1016/j.conbuildmat.2018.04.115

Zhou, L., Gou, M., & Zhang, H. (2023). Investigation on the applicability of bauxite tailings as fine aggregate to prepare 3D printing mortar. *Construction and Building Materials*. https://doi.org/10.1016/j.conbuildmat.2022.129904

Publisher's Note

Ms. Nhi Tran received the B.E. (2018) and M.E. (2020) in Civil Engineering from Ho Chi Minh City University of Technology (HCMUT), Vietnam. She is a Lecturer of Faculty of Civil Engineering, Ho Chi Minh City University of Technology (HCMUT). Her research interests include concrete technology and 3D concrete printing.

Dr. Mien Van Tran is an Associate Professor in Civil engineering, received the B.E. (2002) and M.E. (2004) in Civil Engineering from Ho Chi Minh City University of Technology (HCMUT), Vietnam, D.E. (2008) degree in Civil Engineering from Chulalongkorn University, Thailand. He is a Lecturer of Faculty of Civil Engineering, Ho Chi Minh City University of Technology (HCMUT), a member of ACI, ACF and VCA. His research interests include concrete technology, durability of concrete in aggressive media and 3D concrete printing.

Dr. Phuong Tran is an Associate Professor in Civil engineering, received the M.Sci. (2007) and PhD. (2010) degree in Theoretical & Applied Mechanics from University of Illinois, Urbana Champaign, USA. He is a Lecturer of Faculty Civil & Infrastructure Engineering, RMIT University, Australia. His research interests include 3D concrete printing and modelling of material mechanics.

Mr. An Khanh Nguyen received the B.E. (2023) in Civil Engineering from Ho Chi Minh City University of Technology (HCMUT), Vietnam. His research interests include concrete technology and 3D concrete printing.

Mr. Cuong Quoc Nguyen received the B.E. (2023) in Civil Engineering from Ho Chi Minh City University of Technology (HCMUT), Vietnam. His research interests include concrete technology and 3D concrete printing.